International Journal of Nanomedicine

Dovepress
open access to scientific and medical research

Open Access Full Text Article

ORIGINAL RESEARCH

An Oxygen Supply Strategy for Sonodynamic Therapy in Tuberculous Granuloma Lesions Using a Catalase-Loaded Nanoplatform

Can Hu[1,2,*], Yan Qiu[1,2,*], Jiajun Guo[1,2], Yuchao Cao[1,2], Dairong Li[3], Yonghong Du[1,2]

[1]State Key Laboratory of Ultrasound in Medicine and Engineering, College of Biomedical Engineering, Chongqing Medical University, Chongqing, 400016, People's Republic of China; [2]Chongqing Key Laboratory of Biomedical Engineering, Chongqing Medical University, Chongqing, 400016, People's Republic of China; [3]Department of Respiratory and Critical Care Medicine, the First Affiliated Hospital of Chongqing Medical University, Chongqing, 400016, People's Republic of China

*These authors contributed equally to this work

Correspondence: Dairong Li, Department of Respiratory and Critical Care Medicine, the First Affiliated Hospital of Chongqing Medical University, No. 1, Youyi Road, Yuzhong District, Chongqing, 400016, People's Republic of China, Tel +86-23-89012745, Fax +86-23-68485021, Email lidairong@hospital.cqmu.edu.cn; Yonghong Du, State Key Laboratory of Ultrasound in Medicine and Engineering, College of Biomedical Engineering, Chongqing Medical University, No. 1, Yixueyuan Road, Yuzhong District, Chongqing, 400016, People's Republic of China, Tel/Fax +86-23-68485021, Email duyonghong@cqmu.edu.cn

Purpose: Tuberculosis (TB) is a chronic disease caused by *Mycobacterium tuberculosis* (*MTB*) that remains a major global health challenge. One of the main obstacles to effective treatment is the heterogeneous microenvironment of TB granulomas. This study aimed to investigate the potential of a hypoxic remission-based strategy to enhance the outcome of tuberculosis treatment when implemented in combination with ultrasound.

Methods: A PLGA nanoparticle (LEV@CAT-NPs) loaded with levofloxacin (LEV) and catalase (CAT) was fabricated by a double emulsification method, and its physical characteristics, oxygen production capacity, drug release capacity, and biosafety were thoroughly investigated. The synergistic therapeutic effects of ultrasound (US)-mediated LEV@CAT-NPs were evaluated using an experimental mouse model of subcutaneous tuberculosis granuloma induced by *Bacille Calmette-Guérin* (*BCG*) as a substitute for *MTB*.

Results: LEV@CAT-NPs exhibited excellent oxygen production capacity, biosafety, and biocompatibility. Histological analysis revealed that ultrasound-mediated LEV@CAT-NPs could effectively remove bacteria from tuberculous granulomas, significantly alleviate the hypoxia state, reduce the necrotic area and inflammatory cells within the granuloma, and increase the penetration of dyes in granuloma tissues. The combined treatment also reduced the serum levels of inflammatory cytokines (eg, TNF-α, IL-6, and IL-8), and significantly downregulated the expression of hypoxia-inducible factor 1α (HIF-1α) and vascular endothelial growth factor (VEGF). These results suggested that the synergistic treatment of ultrasound-mediated LEV@CAT-NPs effectively eradicated the bacterial infection and reversed the hypoxic microenvironment of tuberculous granulomas, further promoting tissue repair.

Conclusion: This study provides a non-invasive and new avenue for treating refractory tuberculosis infections. The potential role of regulating hypoxia within infected lesions as a therapeutic target for infection deserves further exploration in future studies.

Keywords: tuberculosis granulomatous, hypoxia, catalase, sonodynamic therapy, *Bacille Calmette-Guérin*

Introduction

Tuberculosis (TB) is an infectious disease caused by *Mycobacterium tuberculosis* (*MTB*). It can cause chronic granulomatous lesions in various parts of the body,[1] and it ranks as the leading cause of death from a single microbial pathogen worldwide. Previous studies have shown that treating TB can be difficult due to poor antibiotic penetration into the granulomas where the bacteria reside.[2] The World Health Organization recommends a six-month combination therapy of four first-line antituberculosis drugs as the standard treatment for TB.[3] However, despite global efforts, the success rate of TB treatment remains unsatisfactory.

Received: 4 August 2023
Accepted: 11 October 2023
Published: 2 November 2023

The tuberculous granuloma, a hallmark structure of tuberculosis, has long been thought to be impenetrable and restrict mycobacterial infection.[4] Recently, real-time imaging technology has revealed that the tuberculous granuloma is a highly complex and dynamic lesion.[5] It not only limits the spread of *MTB* and isolates infection, but also provides a niche for *MTB* growth. The granuloma microenvironment, which includes necrosis, fibrosis, hypoxia, and pathological angiogenesis, is formed by the mutual shaping of the pathogen and the host.[6]

Innovative research is necessary to address the challenges posed by the abnormal granuloma microenvironment in TB treatment. Hypoxia is thought to be a prominent feature of a well-organized granuloma and occurs in the center of the granuloma.[7] Similarities between TB granulomas and solid cancerous tumors exist, with the abnormal granuloma-associated vasculature contributing to the abnormal granuloma microenvironment.[8] Pathological angiogenesis in granulomas is promoted by the overproduction of hypoxia-inducing factor 1α (HIF-1α) and vascular endothelial growth factor (VEGF) when oxygen cannot be transported to the core of the granuloma.[9] The vascular system surrounding the granuloma is abundant but has a disrupted structure, leading to poor perfusion, restricted penetration of oxygen and drugs into the central area of the lesion, and prolongation of treatment duration.[10–12] Very few studies have assessed the effect of a combination strategy based on oxygen supply on tuberculosis treatment.

Sonodynamic therapy (SDT) is a non-invasive treatment with strong tissue penetration that has shown promising application prospects in the treatment of bacterial infections and tumors.[13,14] SDT works by activating a sonosensitizer with low-intensity ultrasound, which produces reactive oxygen species (ROS) to kill tumor cells and bacteria.[15,16] Our previous study confirmed that ultrasound alone could enhance antibiotic penetration through the cell wall and increase the sensitivity of mycobacteria.[17] However, the therapeutic effect of SDT is severely limited by hypoxia in the microenvironment of the lesion.

Our study proposes a new approach to improving the anti-tuberculosis efficacy of SDT by encapsulating levofloxacin (LEV) and catalase (CAT) in PLGA nanoparticles and combining them with ultrasound to reverse the anoxic microenvironment of tuberculous granulomas. CAT plays a crucial role in catalyzing the conversion from hydrogen peroxide (H_2O_2) in the lesion to oxygen (O_2) and H_2O,[18] thereby alleviating the hypoxic level of the granulomas. Improved hypoxia can downregulate the expression of HIF-1α and VEGF, ultimately facilitating the normalization of vascular structure and function within tuberculous granulomas. LEV is a second-line tuberculosis drug with acoustic sensitivity.[19] By encapsulating both LEV and CAT in PLGA nanoparticles, we aim to address their respective limitations. CAT is easily eliminated from circulation, limiting its practical application.[20] The higher oral dose and poor penetration capacity of LEV in TB lesions led to an increased chance of drug side effects and drug resistance.[21,22] This approach builds on the innovative use of oxygen-carrying nanosystems and catalytic nanoparticles, which have been shown to improve the therapeutic effect of SDT in other studies.[23,24] For example, nanoparticles encapsulated with hemoglobin have improved SDT efficacy against methicillin-resistant *Staphylococcus aureus* myositis,[25] while catalase-based nanomaterials have reversed the tumor hypoxic microenvironment to improve the antitumor efficacy of SDT.[26]

This study successfully fabricated composite nanoparticles (LEV@CAT-NPs) for ultrasound-mediated sonodynamic therapy of tuberculous granuloma induced by *Bacille Calmette-Guérin* (*BCG*) as a substitute for *MTB*. It is a common research method to use the attenuated TB vaccine strain *BCG* as a surrogate for pathogenic *MTB* since there is a high degree of genome identity and a similar growth cycle.[27] The use of these nanoparticles was found to be beneficial in enhancing in vivo SDT therapeutic performance. Moreover, the combined treatment was also effective in "normalizing" the vasculature, thereby reducing hypoxia and improving small-molecule delivery. It is noteworthy that the relationship between oxygen supply, HIF-1α, and VEGF may play a critical role in regulating blood vessel formation for enhancing drug delivery. The treatment principle scheme of ultrasound-mediated LEV@CAT-NPs for sonodynamic therapy of subcutaneous tuberculous granulomas is shown in Scheme 1.

Materials and Methods

Materials

Poly (lactic-co-glycolic acid)-poly (ethylene glycol)-carboxylic acid (PLGA-PEG-COOH, 50:50, MW 15000) copolymer was customized by Jinan Daigang Biotechnology Co., Ltd. Chloroform ($CHCl_3$, MW 119.38) and isopropyl alcohol (MW 60.10) were acquired from Chongqing Chuandong Co., Ltd. Levofloxacin (LEV) powder (98.0% purity), polyvinyl

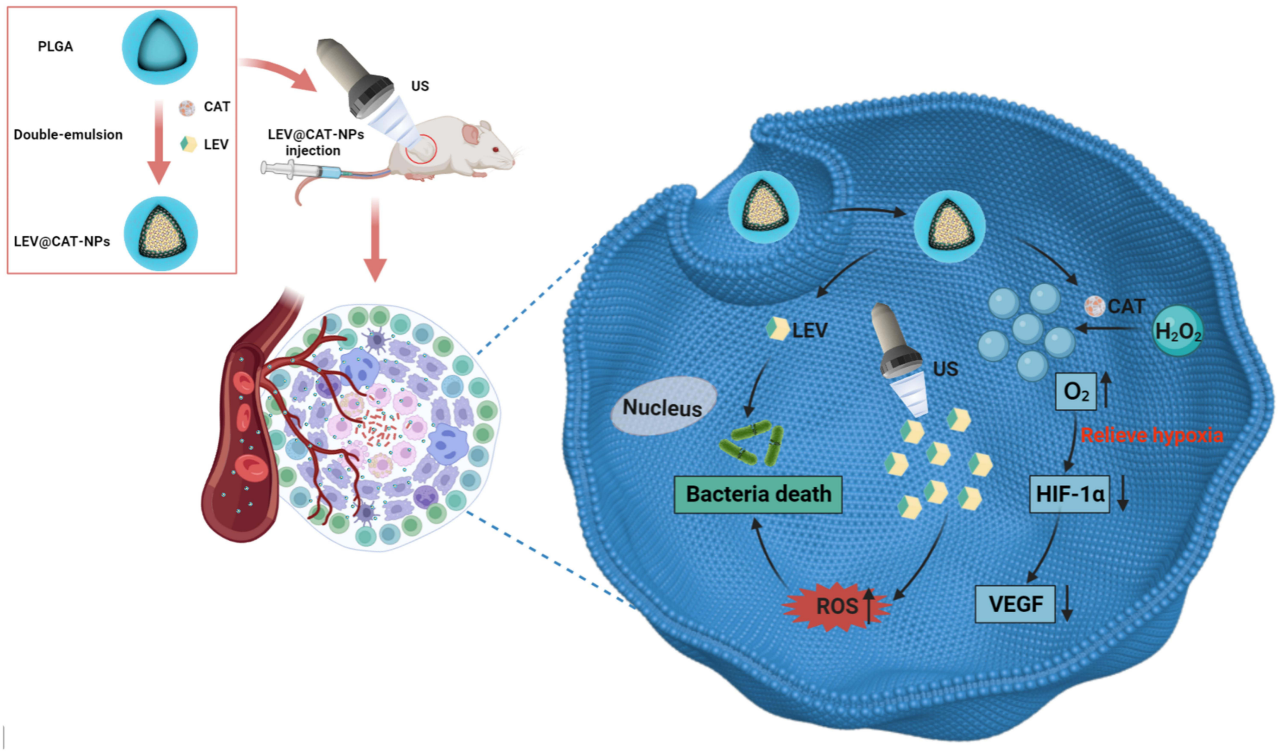

Scheme 1 Scheme illustration of ultrasound-mediated LEV@CAT-NPs for sonodynamic therapy in a mouse model of subcutaneous tuberculosis granuloma infected with *BCG*.

alcohol (PVA, MW30000-70000), SYBR Green II, and dialysis bags were purchased from Sigma-Aldrich (St. Louis, MO, USA). Catalase (CAT) powder (98.0% purity) was obtained from Solarbio Technology Co., Ltd. (Beijing, China). Middlebrook's 7H9 broth medium, Middlebrook's 7H10 agar medium and oleic acid-albumin-dextrose-catalase (OADC) were obtained from BD Biosciences (New York, USA). 2.7-dichlorodihy-drofluorescein diacetate (DCFH-DA) was bought from Beyotime Biotechnology Co., Ltd. (Shanghai, China). Optimum cutting temperature (OCT) compound was acquired from Sakura Finetek USA Inc. Singlet Oxygen Sensor Green (SOSG) and aminophenyl fluorescein (APF) were supplied by Thermo Fisher Scientific (Massachusetts, USA). The H_2O_2 fluorescence assay kit was purchased from AAT Bioquest, Inc. The solid pimonidazole HCl (Hypoxyprobe-1) and affinity-purified rabbit anti-pimonidazole antibody were purchased from Bride Biotechnology Co., Ltd. (Beijing, China). ELISA kits for HIF-1α, VEGF, CD31, α-SMA, TNF-α, IFN-γ, IL-6, and IL-8 were acquired from Jingmei Biotechnology Co., Ltd. (Jiangsu, China).

Microbial Strains and Culture

Bacillus Calmette-Guérin (*BCG*, Batch No. S20013057) was obtained from the Chengdu Institute of Biological Products, Chengdu, China. The cryopreservation bacterial solution was inoculated into 7H9 broth medium supplemented with 0.2% glycerin, 10% Middlebrook OADC, and 0.05% Tween-80 and cultured for three weeks at 37°C and 180 rpm. Then, bacteria were collected by centrifugation and resuspended in Middlebrook's 7H9 broth without Tween-80, and the bacterial concentration was adjusted to 2.0×10^8 CFU/mL for future experiments.

Animals

Healthy female BABL/c mice (6–8 weeks old and weighing 18–24 g) were purchased from Chongqing Enswell Biotechnology Co., Ltd., and raised in the IVC2 animal room of the Animal Experiment Center of Chongqing Medical University (Chongqing, China). All procedures involving animals in this study comply with the ethical standards formulated by the Experimental Animal Ethics Committee of Chongqing Medical University (NO. 2022154).

Preparation and Characterization of Drug-Loaded Nanoparticles

LEV@CAT-NPs were prepared using a double emulsification method similar to the one we previously described.[28] Briefly, the PLGA-PEG-COOH copolymer (40 mg) was immediately mixed with LEV solution (10 mg/mL, 100 μL) and CAT solution (1 mg/mL, 100 μL) after being fully dissolved in $CHCl_3$ (2 mL). Subsequently, the above mixture was emulsified twice in an ice bath with the ultrasonic probe (XL2020 Acoustic Vibrograph, USA) at an intensity of 105 W to obtain colostrum and compound emulsion, respectively. The two emulsification times were 2 minutes and 5 minutes, respectively. Before the second emulsification, it is necessary to add the PVA solution (4%, 4 mL) into the above colostrum to form a complex emulsion. Afterward, to remove $CHCl_3$ from the complex emulsion, isopropyl alcohol (2%, 6 mL) was added to the complex emulsion and stirred at 150 rpm for 3 hours using a magnetic stirrer. Finally, LEV@CAT-NPs were separated by centrifugation (8000 rpm for 10 minutes) and washed twice with distilled water. Deionized water-loaded nanoparticles (Blank-NPs), levofloxacin-loaded nanoparticles (LEV-NPs), catalase-loaded nanoparticles (CAT-NPs), and DiR-loaded nanoparticles (DiR-NPs) were created using the same method, but LEV and CAT solutions were swapped out for equal amounts of deionized water, LEV solution, CAT solution, or DiR solution. The prepared nanoparticles were then freeze-dried and stored.

The average diameter, zeta potential, and polydispersity index (PDI) of nanoparticles were measured by the Malvern laser granularity instrument (Zeta SIZER 3000HS, America). The surface morphology and microstructure of LEV@CAT-NPs were observed by scanning electron microscopy (SEM, Hitachi S-3400N, Japan) and transmission electron microscopy (TEM, Hitachi H-7600, Japan). The LEV@CAT-NPs were dispersed in PBS, and the change in particle size was measured over a period of 7 days to evaluate the stability of the nanoparticles. The drug loading content (LC%) and the encapsulation efficiency (EE%) of LEV and CAT in LEV@CAT-NPs were determined by a UV-vis spectrophotometer (UV-2600, Shimadzu, Japan). The LC% and EE% of the drugs (LEV and CAT) in LEV@CAT-NPs were calculated using the following equations:

$$\text{LC (\% w/w)} = [\text{mass of drug in NPs} / \text{mass of loaded NPs recovered}] \times 100\%,$$

$$\text{EE (\% w/w)} = [\text{mass of drug in NPs} / \text{amount of drug used in encapsulation}] \times 100\%.$$

In vitro Drug Release Experiments Under Ultrasonic Stimulation

The dialysis method in vitro was used to evaluate the drug release kinetics of nanoparticles with or without ultrasound stimulation.[29] LEV@CAT-NPs (20 mg) were dissolved in a phosphate buffered solution (PBS, 2 mL). The mixture was subjected to 1.0 MHz, 1.2 W/cm^2, and 3 minutes of ultrasonic irradiation and then transferred into a dialysis bag, which was soaked in PBS (25 mL) with stirring at 120 rpm for dialysis. The LEV and CAT concentrations of each sample were detected at several predetermined time periods (0, 2, 4, 6, 8, 10, 12, 24, 36, 48, 60, and 72 hours) by using a UV-vis spectrophotometer at the wavelengths of 303 nm and 280 nm, respectively. In the experimental group without ultrasound irradiation, the nanoparticle sample (LEV@CAT-NPs) was transferred to the dialysis bag immediately after it was completely dissolved in PBS. All other procedures were conducted consistent with the ultrasound-irradiated experimental group. The cumulative drug (LEV and CAT) releases (%) were calculated according to the following equation:

Cumulative release of drug (%) = (amount of drug in PBS solution / total drug in LEV@CAT-NPs) ×100%.

Evaluation of Oxygen Generation

LEV@CAT-NPs with CAT-mimic activity could decompose H_2O_2 to produce O_2. The amount of dissolved O_2 in each reaction solution was measured by a portable dissolved oxygen meter (JPB-607A, Shanghai, China). In brief, an equal volume of the different solutions containing either free LEV, free CAT, LEV-NPs, CAT-NPs, or LEV@CAT-NPs (the final concentrations of LEV and CAT were 0.5 mg/mL and 0.1 mg/mL, respectively) were added to a 3% H_2O_2 solution, where distilled water was mixed with H_2O_2 as a negative control for the test. Then, the amount of O_2 generation in each reaction solution was measured by a portable dissolved oxygen meter in real time. Meanwhile, the formation of O_2 bubbles in the reaction solution was observed and photographed.

CAT Activity and Stability Assays in LEV@CAT-NPs

The activity of CAT in LEV@CAT-NPs was measured by the ammonium molybdate method.[30] H_2O_2 reacted with ammonium molybdate to form a stable yellow complex with a strong absorption peak at 405 nm. First, H_2O_2 (30 μM, 100 μL) was mixed with the different solutions containing either free CAT, CAT-NPs, or LEV@CAT-NPs (the final concentrations of LEV and CAT were 0.5 mg/mL and 0.1 mg/mL, respectively) and accurately reacted in a water bath at 25°C for 10 minutes. Subsequently, ammonium molybdate (180 μL) was added to the resulting mixture and incubated for 10 minutes at room temperature. Finally, the absorbance value of the reaction solution at 405 nm was measured by the microplate reader instrument (Infinite M200 Pro N, Tecan, Switzerland), and the catalytic activity of CAT in LEV@CAT-NPs was calculated.

To assess the anti-proteolytic activity of CAT in nanoparticles, an equal volume of the different solutions containing either free CAT, CAT-NPs, or LEV@CAT-NPs (the final concentration of CAT was 0.1 mg/mL) was incubated with proteinase K (0.5 mg/mL) at 37°C. Then, the activity of CAT in nanoparticles was detected using the ammonium molybdate method mentioned above after 12 or 24 hours of proteinase K treatment.

Ultrasound-Mediated LEV@CAT-NPs Synergistic Therapy in vivo

A model of subcutaneous tuberculous granuloma in *BCG*-infected mice was successfully established by subcutaneous injection of a bacterial suspension (Supplementary Material 1 and Figure S1). The mice bearing subcutaneous tuberculous granulomas were divided into eight groups at random (n = 5/group) and given different treatments, respectively. Treatments included the following: (1) sterile saline solution without ultrasound treatment (control), (2) sterile saline solution with ultrasound treatment (US), (3) LEV alone treatment (LEV), (4) LEV-NPs alone treatment (LEV-NPs), (5) LEV@CAT-NPs alone treatment (LEV@CAT-NPs), (6) LEV with ultrasound treatment (US+LEV), (7) LEV-NPs with ultrasound treatment (US+LEV-NPs), and (8) LEV@CAT-NPs with ultrasound treatment (US+LEV@CAT-NPs). For in vivo administration, mice received tail vein injections with a dose of 200 μL sterile saline solution or the suspension of different NPs (the corresponding concentrations for LEV and CAT are 0.5 mg/mL and 0.1 mg/mL, based on a clinically appropriate dose and existing literature reports)[18,31] once every three days for 12 days. The in vivo biodistribution results showed that LEV@CAT-NPs were able to effectively accumulate at the granuloma site and reached a peak 24 hours after injection (Supplementary Material 2 and Figure S2). Therefore, animals were not subjected to ultrasound irradiation until 24 hours after intravenous administration of the appropriate drug preparation or saline. The ultrasound irradiation parameters (a frequency of 1 MHz and a power of 1.2 W/cm^2 for 3 minutes) were determined based on the safety results of ultrasound percutaneous irradiation of mice (Supplementary Material 3 and Figure S3).

The long (A) and short (B) diameters of the subcutaneous granuloma in each mouse were recorded with a vernier caliper every two days for a total of 14 days. The volume of the granuloma was calculated by the formula ($A \times B^2/2$). After 14 days of treatment, the orbital blood of mice was collected to detect changes in the levels of pro-angiogenic and anti-inflammatory factors, as well as indexes of liver and kidney function. Then, the mice were euthanized at the end of a 14-day treatment period, and granuloma tissues were collected for H&E staining, immunohistochemical staining, and bacterial colony enumeration. The major organs were removed and analyzed using H&E staining for the biosafety assessment of LEV@CAT-NPs.

Bacterial Colony-Forming Units (CFU) Analysis

Bacterial CFU were quantified by plating triplicate serial 10-fold dilutions of the tissue homogenate on Middlebrook's 7H10 agar plates. The agar plates were incubated at 37°C for three weeks, and bacterial colony count analysis was expressed as log10 CFU per gram of tissue ($\log_{10}$ CFU/g).

Determination of the H_2O_2 Level in the Granulomatous Tissue

On the 14th day after treatment with different methods, granuloma tissue from experimental animals was aseptically removed and homogenized on ice. The supernatant was collected for subsequent assays after centrifugation, and the concentration of H_2O_2 in the supernatant was measured using a hydrogen peroxide assay kit (Beyotime Biotechnology Co., Ltd., Shanghai, China) according to the manufacturer's instructions.

Measurement of Hypoxia Within the Granulomatous Tissue

The mice were intraperitoneally injected with pimonidazole solution (1.5 mg/kg) on the 14th day after the completion of different treatment modalities. After observation for 60 minutes, the mice were euthanized by cervical dislocation, and granuloma tissue was removed and fixed with 4% paraformaldehyde to prepare paraffin sections. Tissue sections were incubated with the rabbit anti-pimonidazole antibody (Hypoxyprobe^{TM} Omni Kit, Bride Biotechnology Co., Ltd., Beijing, China), and the anoxic extent of the granulomatous tissue was observed by an optical microscope (Olympus, Canada) and quantified by Image J software (National Institutes of Health).

Immunohistochemistry Analysis

Slices of sectioned granuloma tissue were treated with sodium citrate to restore the antigen and incubated with primary antibodies against HIF-1α and VEGF overnight at 4°C. The sections were then treated with a reaction enhancement solution, secondary antibodies, and DAB matrix. Tissue sections were also stained with CD31 and α-SMA immunofluorescence.

ELISA Test

After 14 days of treatment, mouse blood was collected, centrifuged, and the supernatant stored at −80°C until use. The supernatant was then used to quantify angiogenesis-related factors (HIF-1α, VEGF, CD31, and α-SMA) and inflammatory cytokines (IFN-γ, TNF-α, IL-6, and IL-8) using ELISA kits according to the manufacturer's instructions.

Detection of Oxidative Stress in the Granulomatous Tissue

On the 14th day following experimental animal therapy, granuloma tissues from the mice were obtained and homogenized with lysate on ice. The supernatant was collected by centrifugation and then used to detect the activity of peroxide and antioxidant enzymes using MDA and SOD kits (Abbkine Scientific Co., Ltd., Wuhan, China) according to the manufacturer's instructions, respectively.

Evans Blue Dye Extravasation Assay

In this work, vascular permeability in granuloma tissue was measured using Evans blue (EB) dye extravasation. Mice from each group received a tail vein injection of EB dye (at a concentration of 0.5% and a dose of 200 μL). After the mice were put to death 60 minutes post-injection, the granuloma tissue was collected, weighed, and submerged in a formamide solution (1 mL) to prepare tissue homogenate, and then incubated in a 55°C constant-temperature water bath for 48 hours to extract EB from the tissue. After centrifugation at 3000 rpm for 5 minutes, the supernatant was kept, and the absorbance value at 620 nm was measured with the microplate reader instrument (Infinite M200 Pro N, Tecan, Switzerland). The exudation of EB in the unit granuloma tissue was calculated using the standard curve equation (Y = 0.1147X-0.01265, R^2 = 0.9977, where Y is the absorbance value at 620 nm and X is the EB concentration) and the following formula:

Exudation of EB (μg/g) = concentration of EB in supernatant (mg/mL) × 1 / weight of granuloma tissue (mg), wherein 1 represents the volume of formamide solution used to extract EB dye from tissues.

Investigation of Hoechst33342 Delivery in the Granuloma Tissue

Vascular permeability and vascular structural integrity in the granuloma tissue were also assessed using Hoechst33342 dye (blue fluorescence). After the treatment, mice in all groups received a tail vein injection of Hoechst33342 dye (at a concentration of 10 mg/mL and an injection dose of 0.1 mL/mouse). After the mice were observed for 60 minutes, granuloma tissue was removed, embedded in OCT compound, frozen, and stained with SYBR Green II (green fluorescence) to assess vascular permeability by CLSM observation.

Statistical Analysis

The experimental data in this study were described as the mean ± standard deviation (SD) (X ± SD), and statistical analysis was performed using GraphPad Prism version 8 (GraphPad Software; La Jolla, CA, USA). The *t*-test was used for comparisons between two groups, while the one-way ANOVA was used for comparisons among multiple groups. The results were considered significantly different when $p < 0.05$. *, $p < 0.05$, **, $p < 0.01$, and ***, $p < 0.001$.

Results and Discussion

Characterization of Nanoparticles

The physicochemical properties and morphology of the fabricated nanoparticles were summarized in Table 1 and Figure 1. The SEM and TEM images of the prepared LEV@CAT-NPs revealed a spherical morphology with uniform particle size and good monodispersity (Figure 1A and B). Furthermore, the mean size of LEV@CAT-NPs remained relatively consistent in PBS at 37°C within seven days (Figure 1C), which demonstrated the high stability of LEV@CAT-NPs and the potential for further in vivo studies. Besides, the absorption peak of the LEV@CAT-NPs overlapped with that of the drug LEV or CAT, which indicated that the LEV and CAT were successfully encapsulated into the nanoplatform (Figure 1D). The average diameter of the LEV@CAT-NPs was (335.00 ± 14.68) nm with a PDI of (0.20 ± 0.02), which did not significantly increase compared with Blank-NPs (266.80 ± 5.77) nm. The mean zeta potentials of LEV@CAT-NPs were (−9.64 ± 0.68) mV, while those of Blank-NPs were (−15.30 ± 0.46) mV (Table 1), indicating that the optimal size and negative surface charge of NPs promote their efficient aggregation in tuberculous granuloma tissue sites, similar to the passive enhanced permeability and retention (EPR) effect observed in tumors.[32] The drug encapsulation efficiency and loading content of LEV and CAT in LEV@CAT-NPs were 63.51 ± 1.07% (LEV), 57.67 ± 0.62% (CAT), 3.59 ± 0.12% (LEV), and 1.63 ± 0.06% (CAT), respectively (Table 1).

Next, the drug-releasing capacity of the LEV@CAT-NPs delivery system triggered by ultrasound was evaluated using the dialysis bag method. As shown in Figure 1E, the LEV@CAT-NPs released LEV (49.73%) and CAT (46.67%) sharply within the first 36 hours of stimulation by ultrasound exposure, and the cumulative concentrations of LEV and CAT increased significantly within 72 hours compared to the non-ultrasound exposure group, reaching a total release rate of 69.18% and 70.37%, respectively. This demonstrated that LEV@CAT-NPs' releasing behavior could be mediated by ultrasound exposure.

Investigation of the Oxygen Release Behavior and Enzyme Activity of LEV@CAT-NPs

It is generally recognized that CAT is capable of decomposing H_2O_2 into O_2 and H_2O.[33] The ability of LEV@CAT-NPs to catalyze the conversion of H_2O_2 into O_2 is crucial for relieving hypoxia in the microenvironment of tuberculous granulomas in vivo. In this paper, the oxygen production capacity and enzymatic activity of nanoparticles (LEV@CAT-NPs) were investigated. As shown in Figure 1F, after incubation of different samples with 3% H_2O_2, significant oxygen bubble formation was observed in the free CAT, CAT-NPs, and LEV@CAT-NPs groups, while this phenomenon was not observed in the free LEV and LEV-NPs groups, indicating that experimental groups containing CAT were able to trigger the decomposition of H_2O_2 to produce O_2. The amount of dissolved oxygen in each group was further monitored in real time using a portable dissolved oxygen meter, as shown in Figure 1G. The results showed that the free CAT, CAT-NPs, or LEV@CAT-NPs produced higher levels of O_2 within 2 minutes. The consistency between the direct observation of

Table 1 The Physical Characteristics of Nanoparticles

Formulations	Average Size (nm)	Zeta Potential (mV)	PDI	LC (%)	EE (%)
Blank-NPs	266.8 ± 5.77	−15.3 ± 0.46	0.15 ± 0.04	—	—
LEV-NPs	294.2 ± 8.11	−10.8 ± 0.74	0.10 ± 0.07	3.74 ± 0.09	76.29 ± 3.11
CAT-NPs	290.1 ± 9.01	−13.2 ± 0.40	0.15 ± 0.03	2.98 ± 0.15	67.81 ± 1.21
LEV@CAT-NPs	335.0 ± 14.68	−9.64 ± 0.68	0.20 ± 0.02	3.59 ± 0.12[a] 1.63 ± 0.06[b]	63.51 ± 1.07[a] 57.67 ± 0.62[b]

Notes: Blank-NPs, deionized water-loaded PLGA nanoparticles; LEV-NPs, LEV-loaded PLGA nanoparticles; CAT-NPs, CAT-loaded PLGA nanoparticles; LEV@CAT-NPs, LEV and CAT-loaded PLGA nanoparticles; [a], LEV; [b], CAT.
Abbreviations: PDI, polydispersity index; LC, loading content of drug; EE, encapsulation efficiency of drug.

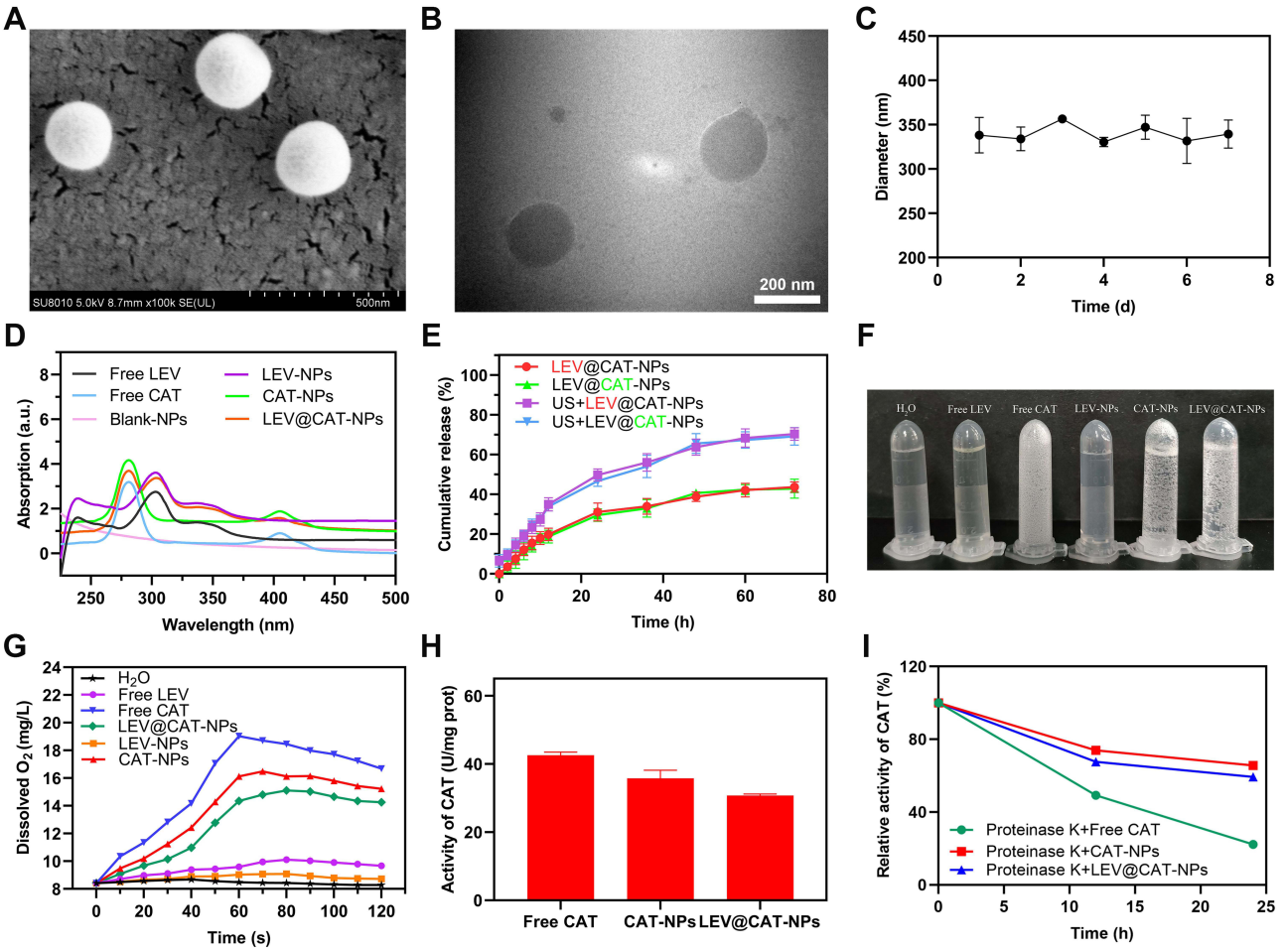

Figure 1 Physical and chemical characterization of the LEV@CAT-NPs. (**A**) SEM image of the LEV@CAT-NPs. The scale bar is 500 nm. (**B**) TEM image of the LEV@CAT-NPs. The scale bar is 200 nm. (**C**) The average size distribution of LEV@CAT-NPs in PBS within 7 days. (**D**) Characteristic peak of the free LEV, free CAT, Blank-NPs, LEV-NPs, CAT-NPs, and LEV@CAT-NPs solution absorbance values at 303 nm or 280 nm as shown by UV-vis spectrophotometry. (**E**) The cumulative LEV and CAT release in the presence or absence of ultrasonic irradiation was examined by a UV-vis spectrophotometer (The red text indicates the cumulative release rate of LEV, while the green text indicates the cumulative release rate of CAT). (**F** and **G**) Photographs of oxygen production (**F**) and a quantitative assay of dissolved oxygen (**G**) were obtained by reacting 3% H_2O_2 with free LEV, free CAT, LEV-NPs, CAT-NPs, and LEV@CAT-NPs solutions. (**H**) Evaluation of enzyme activity for free CAT, CAT-NPs, and LEV@CAT-NPs without proteinase K. (**I**) Relative enzymatic activity of free CAT, CAT-NPs, and LEV@CAT-NPs in the presence of proteinase K at different times. The data represent the mean ± SD of three independent experiments.

bubbles (Figure 1F) and the measurement results obtained using a portable dissolved oxygen meter (Figure 1G) confirmed the catalase-based LEV@CAT-NPs' excellent oxygen production capacity. This ability to produce oxygen is crucial for subsequent experimental research and highlights the potential of LEV@CAT-NPs as a therapeutic strategy for the hypoxic microenvironment of tuberculous granulomas.

Meanwhile, Figure 1H shows that the enzymatic activity of CAT-NPs or LEV@CAT-NPs is somewhat reduced compared to free CAT, possibly due to the low drug-loading content of CAT in nanoparticles or the inability of nanoparticles to fully release CAT. After incubation with proteinase K for 24 hours, free CAT lost most of its enzymatic activity (Figure 1I), while the nanoparticles loaded with CAT (eg, CAT-NPs and LEV@CAT-NPs) maintained a relatively high level of catalytic activity. This finding is consistent with previous reports that nanoparticles can protect catalase from the hydrolysis of external proteases, thus improving its stability.[34]

Synergistic Therapeutic Effect of Ultrasound-Mediated LEV@CAT-NPs in vivo

The in vitro hemolysis and cytotoxicity tests confirmed that LEV@CAT-NPs have excellent safety in vitro, establishing a basis for future in vivo experiments (Supplementary Material 4, Supplementary Material 5, and Figure S4). A typical tuberculous

granuloma structure with severe internal hypoxia was observed through H&E and pimonidazole immunohistochemical staining after 12 days of *BCG* subcutaneous infection (Supplementary Material 1 and Figure S1). Therefore, combined therapy with ultrasound and LEV@CAT-NPs on the subcutaneous tuberculous granuloma of a mouse model was carried out. The schematic diagram of the treatment scheme is shown in Figure 2A. The granulomatous volumes of mice in each group

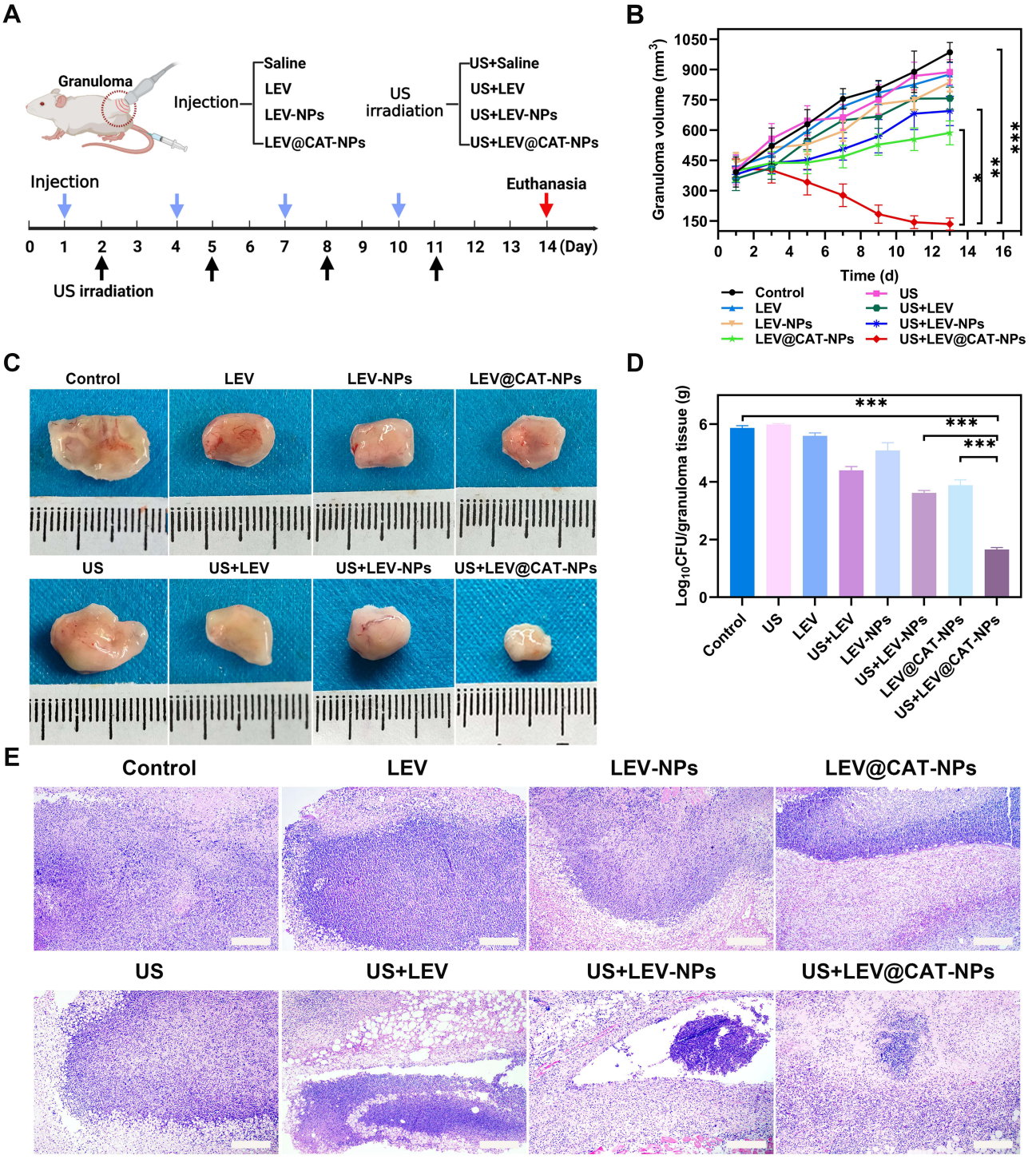

Figure 2 In vivo synergistic effects of ultrasound-mediated LEV@CAT-NPs. (**A**) Treatment protocols of experimental mice with a subcutaneous tuberculosis granuloma. (**B**) Volume change curves of granulomatous tissues in each group of mice during 14 days of treatment by different modalities. (**C**) Photographs of isolated granulomatous tissues after 14 days of treatment with different modalities. (**D**) CFU analysis of bacterial cultures from granulomatous tissues after 14 days of treatment by different modalities. (**E**) H&E staining images of granulomatous tissues after 14 days of treatment with different modalities. The scale bar is 100 μm. The data represent the mean ± SD of three independent experiments. *$p < 0.05$, **$p < 0.01$, ***$p < 0.001$.

were measured every 2 days for 14 days after different treatments, as shown in Figure 2B and 2C. The volume of granulomatous in the US group (977.55 ± 50.68) mm^3 or free LEV group (928.21 ± 38.56) mm^3 increased gradually over the course of 14 days and was very close to those of the control group (1076.63 ± 39.61) $mm,^3$ indicting no obvious inhibition of the growth of granuloma with single free LEV or US. However, the granulomatous volumes following combined therapy of US and LEV@CAT-NPs were considerably lower within 14 days as compared to other treatment groups, demonstrating that US combined with LEV@CAT-NPs had a distinct granuloma growth suppression effect (Figure 2B and C). Furthermore, the numbers of bacterial colonies in the granulomatous tissues were counted on the 14th day post-treatment, as shown in Figure 2D. The US+LEV@CAT-NPs group had the lowest bacterial burden among all groups, suggesting that ultrasound-mediated LEV@CAT-NPs could effectively enhance the injury effect of *BCG* in granulomatous tissue. Previous studies have demonstrated the strong destructive effect of ROS on bacterial DNA.[35] In the production experiment of ROS, it was confirmed that LEV@CAT-NPs could generate more ROS under ultrasonic stimulation (Supplementary Material 6 and Figure S5). Additionally, the cavitation effect and high shear force of ultrasound can significantly disrupt the structural integrity of bacteria.[36] Therefore, the combination of ultrasound with LEV@CAT-NPs results in a more effective bactericidal effect.

Histological analysis showed that the granulomatous tissues of mice following various treatments varied significantly from one another, as shown in Figure 2E. On the 14th day after treatment, the typical histological characteristics of granulomatous tissues caused by *BCG* infection were visible after treatment with sterile saline (control), US alone, or LEV alone. Following treatment with LEV-NPs or LEV@CAT-NPs alone, a marked necrosis in the granulomatous region was also observed, but the area of necrosis was significantly reduced compared with the control. The granuloma area and inflammatory symptoms were reduced in the US+LEV and US+LEV-NPs groups. Particularly, the LEV@CAT-NPs combined with ultrasound treatment completely eliminated the granulomatous structure, focal necrosis, and inflammatory cells. In addition, the in vivo biosafety of LEV@CAT-NPs combined with ultrasound synergistic therapy was confirmed by blood biochemical tests and H&E staining of major organs (Supplementary Material 7 and Figure S6).

Hypoxia Relief in Granulomatous Tissue After Treatment with US+LEV@CAT-NPs

The hypoxic microenvironment of tuberculous granulomas is not only associated with increased TB severity but also provides favorable conditions for the persistence of *MTB*.[37] Immunohistochemical staining with pimonidazole was employed to analyze the effect of different treatments on the extent of hypoxia in granulomatous tissues, as shown in Figure 3A. The results showed that ultrasound-mediated free LEV or LEV-NPs did not significantly relieve hypoxia within the granulomatous tissue compared with LEV or LEV-NPs alone. However, treatment with LEV@CAT-NPs alone or in combination with ultrasound significantly improved granulomatous hypoxia, with the lowest area fraction (2.53 ± 0.82%) of hypoxia observed in the US+LEV@CAT-NPs group (Figure 3C). The study conducted a dissolved oxygen experiment, which demonstrated that LEV@CAT-NPs reacted with 3% H_2O_2 to produce a considerable amount of oxygen, as shown in Figure 1F and G. Furthermore, drug release experiments confirmed that ultrasonic stimulation facilitated the release of drugs from the nanoparticles, as indicated in Figure 1E, thereby increasing the local drug concentration in the lesion. Overall, ultrasound-mediated LEV@CAT-NPs proved to be a more efficient therapeutic approach for alleviating hypoxia within granulomatous tissue.

HIF-1α is widely recognized as an important regulator of hypoxia, with its expression increasing in the center of granulomas when hypoxia occurs.[38] In this study, the levels of HIF-1α in the granulomatous tissue and serum of mice in each experimental group were detected by immunohistochemical staining and ELISA. As shown in Figure 3B, positive staining of HIF-1α in granulomatous tissue after treatment with LEV@CAT-NPs alone or in combination with ultrasound was significantly reduced compared with the LEV-NPs or US+LEV-NPs groups. The HIF-1α ELISA assay further verified that the combined treatment of LEV@CAT-NPs and ultrasound could alleviate tissue hypoxia (Figure 3D).

The concentration of H_2O_2 within the granulomatous tissue was significantly decreased following treatment with LEV@CAT-NPs or ultrasound-mediated LEV@CAT-NPs compared with other treatment groups (Figure 3E). These experimental results indicated that LEV@CAT-NPs could catalyze the endogenous H_2O_2 to generate O_2, leading to an increase in the consumption of H_2O_2 in the tissue.

In summary, the synergistic treatment of LEV@CAT-NPs and ultrasound decreased the level of H_2O_2 in the granuloma tissue, shrank the hypoxic region of the granuloma tissue, and downregulated the expression of HIF-1α,

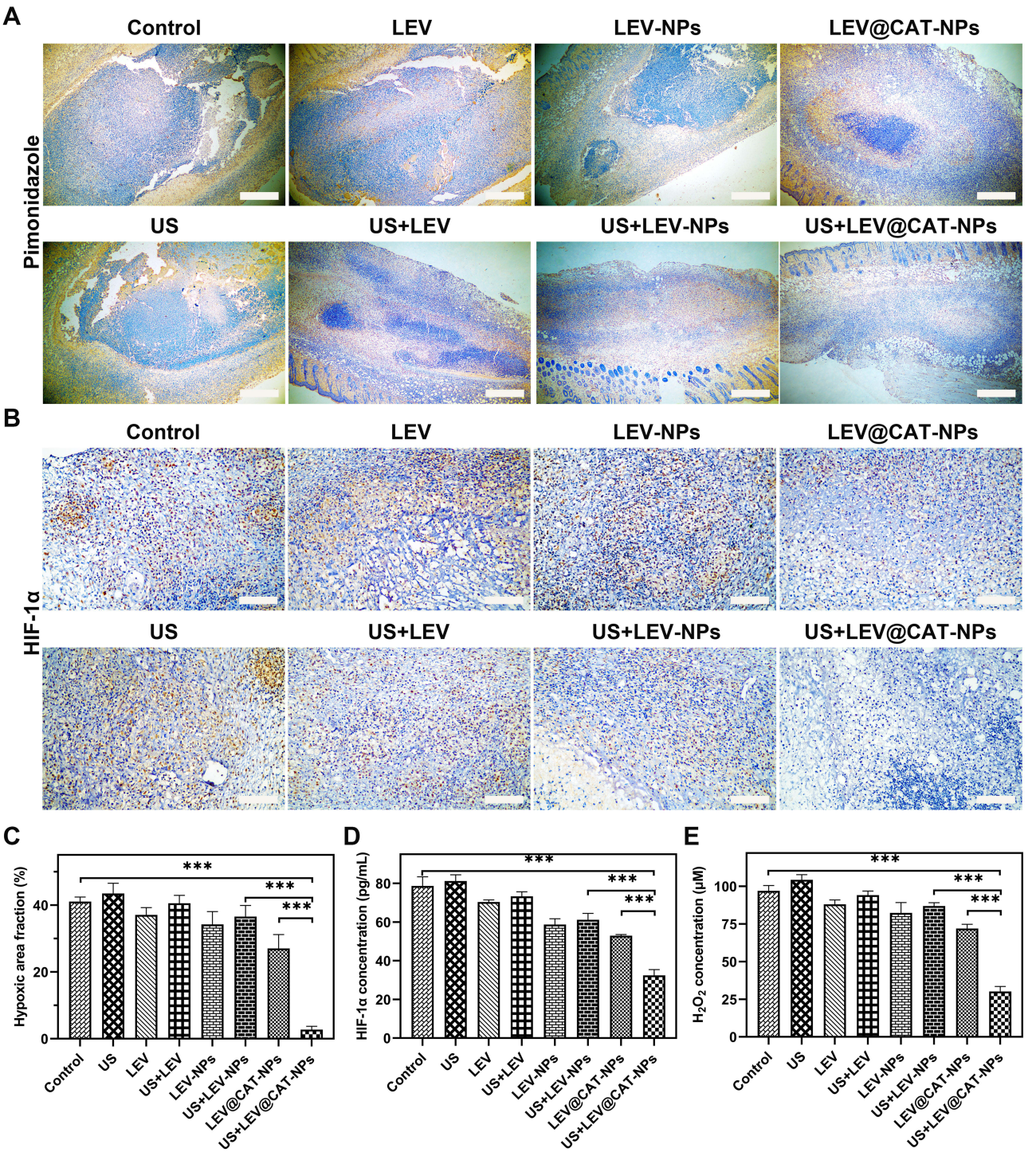

Figure 3 Effect of ultrasound-mediated LEV@CAT-NPs on hypoxia within tuberculous granuloma tissues. (**A**) Images of pimonidazole staining for hypoxia in granulomatous tissue conducted by different treatments. (**B**) Images of HIF-1α immunohistochemical staining in the granulomatous tissue conducted by different treatments. Scale bars are 100 μm. (**C**) Image J quantified the area fraction of hypoxia (brown) within the granulomatous tissue, that is, the brown area of each granuloma area. (**D**) The serum levels of HIF-1α in mice were determined by ELISA with different treatments. (**E**) Level of H_2O_2 within the granulomatous tissue after different treatments. The data represent the mean ± SD of three independent experiments. ***$p < 0.001$.

suggesting that LEV@CAT-NPs catalyzed the endogenous H_2O_2 production of O_2 in the granuloma and alleviated the anoxic state within the granuloma. These findings provide insights into the potential mechanisms underlying the therapeutic effects of LEV@CAT-NPs in combination with ultrasound in targeting the hypoxic microenvironment of tuberculous granulomas.

The US-Mediated LEV@CAT-NPs Combination Therapy Reduced the Expression of VEGF

Mature tuberculous granulomas exhibit abnormal vascular structures, such as disordered arrangements of endothelial cells and a lack of cellular coverage, which lead to insufficient blood flow and exacerbate hypoxia within the granulomas.[39] HIF-1α protein expression is upregulated in hypoxic environments, activating the overexpression of VEGF to cause pathological angiogenesis, resulting in a disorganized vessel network and occluded or embolized blood vessels.[40,41] Ultrasound-mediated LEV or LEV-NPs did not significantly down-regulate the expression of VEGF in granuloma tissue compared with LEV or LEV-NPs alone. However, LEV@CAT-NPs alone or in combination with ultrasound treatment significantly reduced the level of VEGF (Figure 4A). Interestingly, the serum level of VEGF in the US+LEV@CAT-NPs group was the lowest among all treatment groups, approximately half of those in the control group (Figure 4C). Immunohistochemical and ELISA experiments have demonstrated that ultrasound-mediated LEV@CAT-NPs could significantly down-regulate the expression of HIF-1α (Figure 3B and D). Previous studies have reported that VEGF is one of the downstream factors of HIF-1α,[42,43] and the expression of VEGF is notably down-regulated following the treatment of ultrasound combined with LEV@CAT-NPs (Figure 4A and C).

The Combined Treatment of US and LEV@CAT-NPs Reconstructed the Vasculature in the Granuloma Site

The study also evaluated the morphology and structure of the blood vessels in the granuloma tissue using anti-CD31 and anti-α-SMA. The results showed that the red fluorescence of CD31-labeled vascular endothelial cells and the green fluorescence of pericytes labeled with α-SMA in the LEV@CAT-NPs group were significantly increased compared with the LEV or LEV-NPs alone (Figure 4B). Meanwhile, ultrasound in combination with LEV@CAT-NPs significantly increased the density of normal blood vessels compared to other treatments, and the lumen area of blood vessels in the US+LEV@CAT-NPs group was larger than that of other treatment groups (Figure 4B). These findings demonstrated that the synergistic therapeutic effect of ultrasound and LEV@CAT-NPs may promote angiogenesis and improve vascular structure in the granulomatous tissue. Furthermore, serum levels of α-SMA and CD31 in mice treated with LEV@CAT-NPs and US+LEV@CAT-NPs were significantly higher than that in the control group (Figure 4D and E). These results revealed that the combination of ultrasound and LEV@CAT-NPs could "normalize" and reconstruct the vasculature in granulomatous tissues by increasing the density of normal blood vessels and the coverage of pericytes, which may contribute to improved oxygenation and reduced hypoxia in the granulomatous tissue.

Permeability Evaluation of Dyes in Granuloma Tissue Following Treatment of Ultrasound-Mediated LEV@CAT-NPs

Recent research has shown that structural and functional anomalies of the vasculature within granuloma tissue can compromise the delivery and efficacy of anti-tuberculosis medications, leading to a reduced drug supply.[44] This study further analyzed the effect of the synergistic treatment regimen of ultrasound-mediated LEV@CAT-NPs on vascular function (the ability to deliver drugs). Hoechst33342 (with a molecular weight of 615.99 Da) and EB dye as drug models to assess drug delivery in the granuloma. The molecular weight of EB dye itself is 961 Da, and it binds to intravascular serum albumin in vivo to become a protein tracer with a high molecular weight (~67 kDa).[45] CLSM observations found that the delivery of Hoechst33342 (blue fluorescence) in granuloma tissue by the ultrasound combined with LEV@CAT-NPs groups was significantly higher than that of other treatment groups. The blue fluorescent dyes in the US+LEV and US+LEV-NPs groups were mainly distributed around the granuloma tissue, whereas the blue fluorescent dyes in the US +LEV@CAT-NPs group were distributed throughout the tissue (Figure 5A and B). The quantitative results of the EB extravasation assay showed that the amount of EB penetration in the granuloma tissue of the US+LEV@CAT-NPs group was significantly higher than that of the other groups, reaching (124.38 ± 1.62) ug/g (Figure 5C). These results indicated that ultrasound-mediated LEV@CAT-NPs enhance drug delivery in the granuloma tissue.

Our study improves the blood vessels of granulomas through an oxygen supply strategy during SDT, enhances local drug delivery and oxygen, and contributes to sterilization and tissue repair. These findings demonstrated that

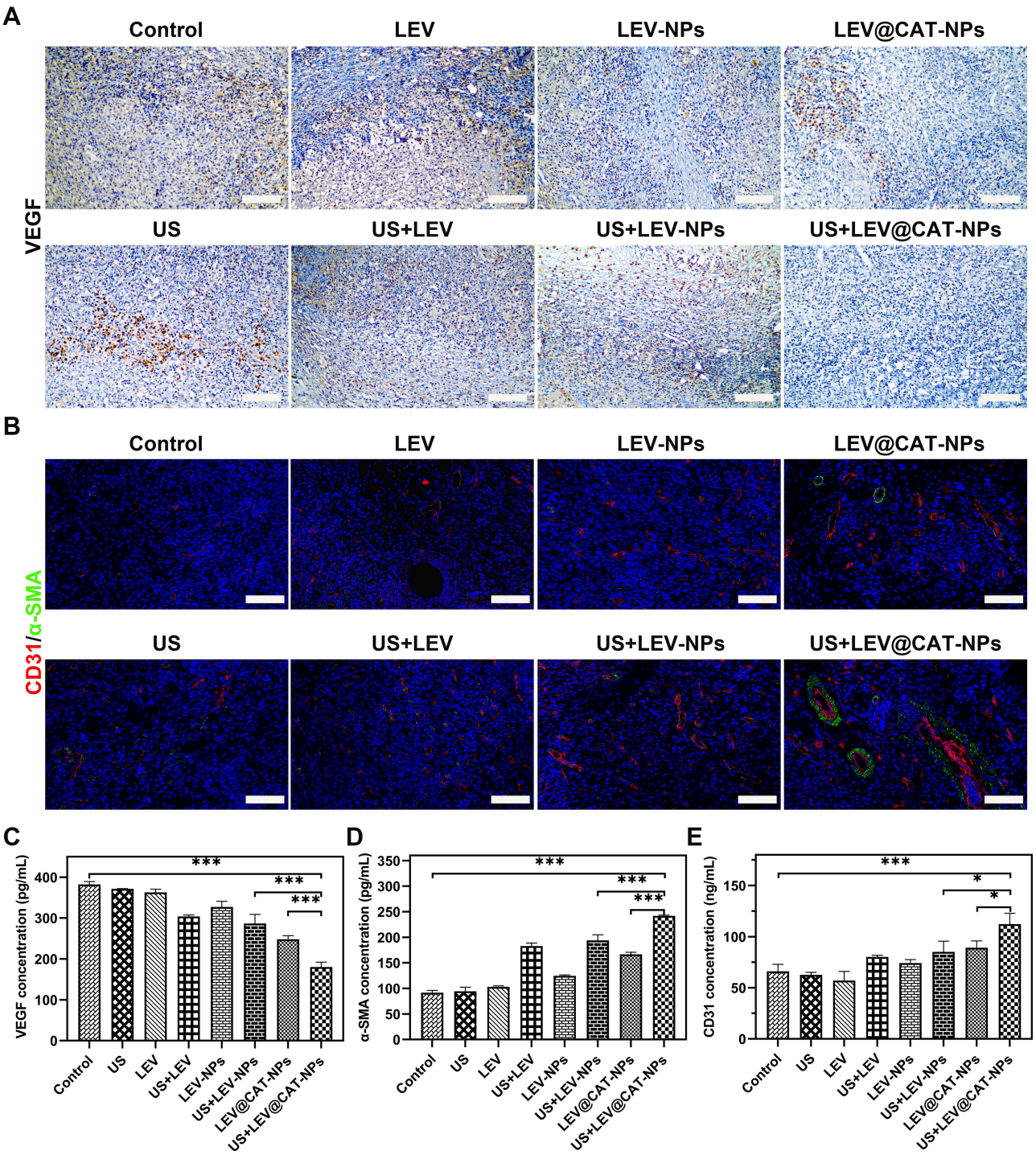

Figure 4 The synergistic effect of ultrasound-mediated LEV@CAT-NPs on the level of angiogenesis-related factors in tissues and serum. (**A** and **B**) Images of immunohistochemical and immunofluorescent staining for VEGF (**A**), α-SMA (**B**), and CD31 (**B**) in the granulomatous tissue conducted by different treatments. Scale bars are 100 μm. (**C**–**E**) Levels of VEGF (**C**), α-SMA (**D**), and CD31 (**E**) in the infected mice were determined by ELISA with different treatments. The data represent the mean ± SD of three independent experiments. *$p < 0.05$, ***$p < 0.001$.

a combination of oxygen supply strategies during SDT could be a promising therapeutic approach for granulomatous diseases.

It is worth noting that MMP inhibitors and an anti-VEGF drug (bevacizumab) have been shown to stabilize blood vessels and enhance the accessibility of drugs to bacteria at the center of the granuloma in *MTB*-infected mice.[8,46] This

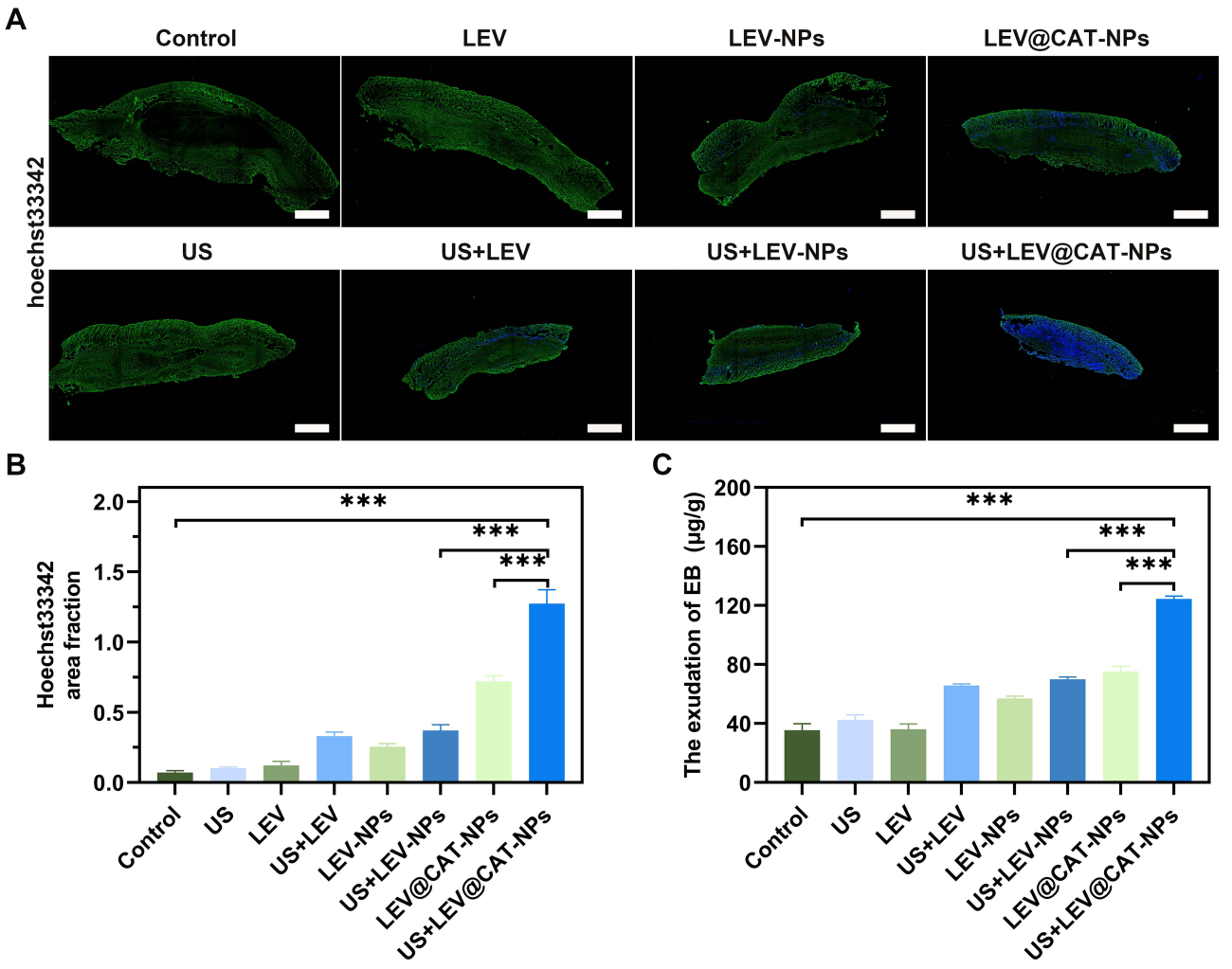

Figure 5 Vascular permeability was detected by dyes with different molecular weights accumulating in granulomatous tissue. (**A**) The distribution of Hoechst33342 in granulomatous tissues was observed by CLSM. The scale bar is 500 μm. (**B**) The area fraction of Hoechst33342 (blue) in granuloma tissue (green) was quantified with Image J. (**C**) The permeability of Evans blue within the granulomatous tissue of infected mice was quantitatively detected. The data represent the mean ± SD of three independent experiments. ***$p < 0.001$.

finding emphasizes the importance of considering vascular structure and function when designing drug delivery strategies for granulomatous diseases. Further research in this area could lead to the development of more effective treatment options for patients with granulomatous diseases.

Levels of Cytokines Following Ultrasound Combined with LEV@CAT-NPs Treatment

The presence of *MTB* breaks the inflammatory homeostasis in the host, further promoting granulomatous lesions and causing irreversible tissue damage, which usually involves the participation of numerous cytokines with different functions.[47,48] The cytokines TNF-α, IL-6, and IL-8 are contributors to the pathogenesis of tuberculosis and are detrimental to host protective immunity.[49] In contrast, IFN-γ mediated host immune responses are highly effective in clearing intracellular pathogens.[50]

To assess the effect of different treatment regimens on cytokine levels, serum levels of TNF-α, IFN-γ, IL-6, and IL-8 were measured in infected mice with granuloma tissue from each group 14 days after therapy. Treatments with LEV, LEV-NPs, LEV@CAT-NPs, US+LEV, US+LEV-NPs, and US+LEV@CAT-NPs all lowered TNF-α, IL-6, and IL-8 levels, with the US+LEV@CAT-NPs group having the best effect (Figure 6A, B, and C). In contrast, IFN-γ levels were further increased after treatment in all groups, especially in the US+LEV@CAT-NPs group, which was significantly

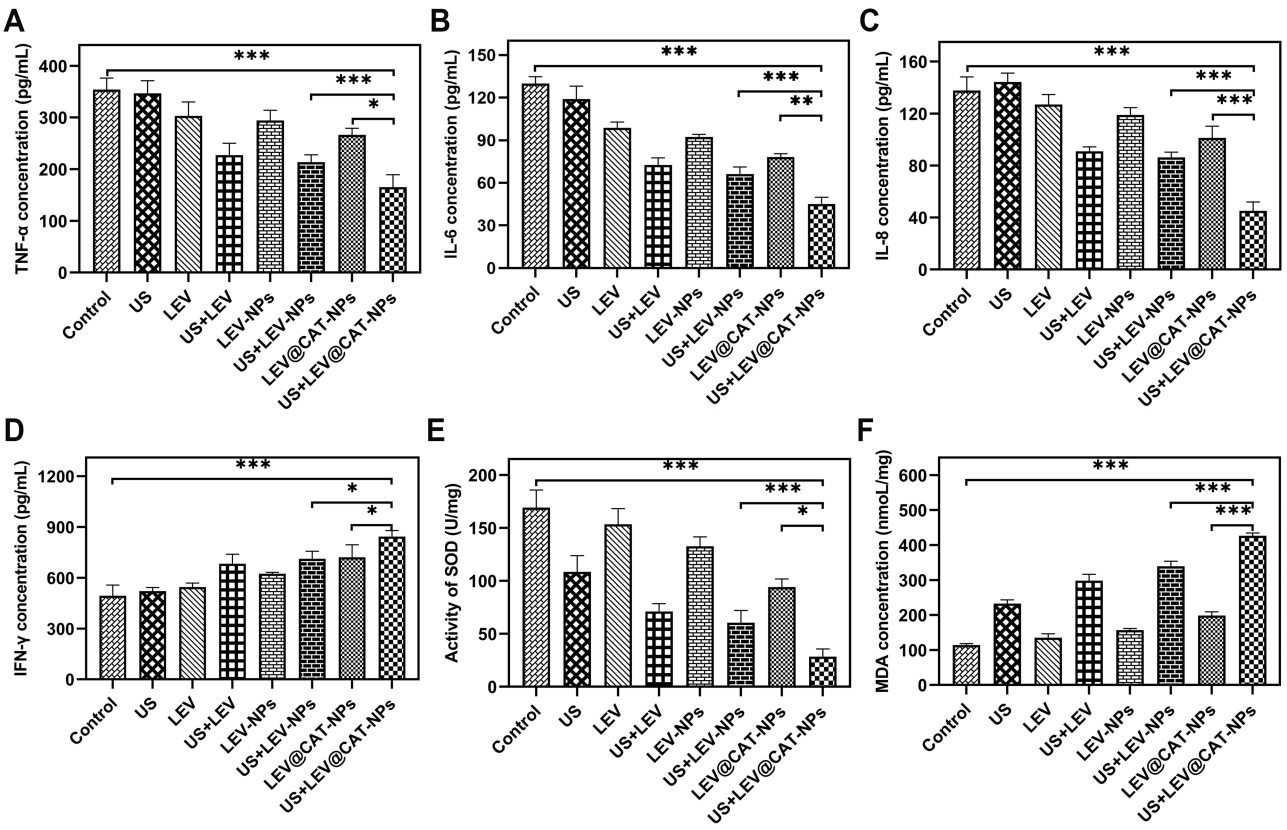

Figure 6 The levels of cytokines and oxidative stress in mice after 14 days of different treatments. (**A**–**D**) The serum levels of TNF-α (**A**), IL-6 (**B**), IL-8 (**C**), and IFN-γ (**D**) in the infected mice after 14 days of different treatments. (**E**) The activities of SOD in the granuloma tissue of infected mice. (**F**) The content of MDA in the granuloma tissue of infected mice. The data represent the mean ± SD of three independent experiments. *p < 0.05, **p < 0.01, ***p < 0.001.

higher than that in the other groups (Figure 6D). The result demonstrated that ultrasound combined with LEV@CAT-NPs treatment of subcutaneous tuberculous granuloma might provide a protective immune response by modulating the immune status of the host, which contributes to the regression of inflammation and thus promotes tissue repair.

The Effect of Ultrasound Combined with LEV@CAT-NPs Treatment on the Oxidative Stress Factors MDA and SOD

Malondialdehyde (MDA) and superoxide dismutase (SOD) are important markers of oxidative stress.[51] MDA is a byproduct of ROS lipid peroxidation, which indirectly measures the level of tissue peroxidation, and SOD is the major antioxidant metalloenzyme that can fend against oxygen-free radicals.[52,53] Supplementary Material 6 and Figure S5A showed that SDT treatment generated significant amounts of ROS. With the therapy of US+LEV@CAT-NPs, it is required to further evaluate the levels of oxidative stress in tissues. Therefore, the content of MDA and the activities of SOD in the tissue were measured to analyze the oxidative stress state in granulomatous tissue. As shown in Figure 6E, the level of SOD in the control group (169.30 ± 13.52) U/mg prot was significantly higher than that in the other groups. Since SOD is an antioxidant enzyme, a low level of SOD suggests that a large amount of ROS could be generated in the granulomatous tissue to kill the internal bacteria. However, the level of SOD (28.34 ± 6.07) U/mg prot in the granuloma tissue was significantly decreased after ultrasound combined with LEV@CAT-NPs treatment. Conversely, the level of MDA in the granulomatous tissue significantly increased nearly twofold after ultrasound combined with LEV, LEV-NPs, and LEV@CAT-NPs compared with LEV, LEV-NPs, and LEV@CAT-NPs treatment alone (Figure 6F). LEV@CAT-NPs were activated by ultrasound in vivo and achieved the bactericidal effect.

Our results show that ultrasound combined with LEV@CAT-NPs treatment induces oxidative stress, as evidenced by an increased level of MDA, accompanied by an increase in ROS such as superoxide radical ($^1O_2$), hydroxyl radical (OH),

and H_2O_2 (Supplementary Material 6 and Figure S5B, C, and D), which cause oxidative stress in biological tissues and cause oxidative damage to bacteria.[54]

Conclusion

The dynamic heterogeneity of tuberculous granulomas poses a challenge to achieving ideal treatment efficacy, as it limits drug permeability in the center of the lesion and leads to drug resistance in *MTB*. In our study, we investigated the use of a combined strategy based on SDT and oxygen supply to address this challenge. Our finding, for the first time to our knowledge, is that this approach effectively alleviated the hypoxia in *BCG*-induced subcutaneous tuberculous granuloma, promoted the normalization of vascular structure within the granuloma tissue, improved the delivery effect of drug model molecules, inhibited the growth of the granuloma, and effectively removed *BCG* from the granuloma tissue.

The potential mechanisms of the synergistic effect of ultrasound-mediated LEV@CAT-NPs may include the following: First, sonodynamic therapy relies on sonochemical oxygen consumption.[55] However, therapeutic efficacy can be impeded by the hypoxic environment of granuloma tissue. To address this issue, our study developed LEV@CAT-NPs. These nanoparticles have the ability to decompose H_2O_2 in situ and generate oxygen, thereby enhancing the effectiveness of SDT. Secondly, under ultrasonic stimulation, LEV@CAT-NPs effectively alleviate hypoxia in granuloma tissue, thereby downregulating the expression of HIF-1α and VEGF. This promotes the normalization of vascular structure, which in turn enhances drug delivery in the granuloma tissues, leading to an improved treatment effect.

Data Sharing Statement

All the data generated in this study is available in the main text or the supplementary materials. The data, analytical methods, and study materials for the purposes of reproducing the results or replicating procedures can be made available on request to the corresponding author who manages the information.

Ethics Approval and Consent to Participate

All procedures involving animals in this study comply with the ethical standards established by the Experimental Animal Ethics Committee of Chongqing Medical University (Ethical Number: 2022154).

Author Contributions

All authors made a significant contribution to the work reported, whether that is in the conception, study design, execution, acquisition of data, analysis and interpretation, or in all these areas; took part in drafting, revising or critically reviewing the article; gave final approval of the version to be published; have agreed on the journal to which the article has been submitted; and agree to be accountable for all aspects of the work.

Funding

This work was supported by the National Natural Science Foundation of China (No. 82270115) and the Chongqing Graduate Research Innovation Project Fund (No. CYS22374).

Disclosure

The authors declare no competing interests in this work.

References

1. Lange C, Chesov D, Heyckendorf J, Leung CC, Udwadia Z, Dheda K. Drug-resistant tuberculosis: an update on disease burden, diagnosis and treatment. *Respirology*. 2018;23(7):656–673. doi:10.1111/resp.13304
2. Arrey F, Löwe D, Kuhlmann S, et al. Humanized mouse model mimicking pathology of human tuberculosis for *in vivo* evaluation of drug regimens. *Front Immunol*. 2019;10:89. doi:10.3389/fimmu.2019.00089
3. Shibeshi W, Sheth AN, Admasu A, Berha AB, Negash Z, Yimer G. Nephrotoxicity and ototoxic symptoms of injectable second-line anti-tubercular drugs among patients treated for MDR-TB in Ethiopia: a retrospective cohort study. *BMC Pharmacol Toxicol*. 2019;20(1):31. doi:10.1186/s40360-019-0313-y
4. Cohen SB, Gern BH, Urdahl KB. The tuberculous granuloma and preexisting immunity. *Annu Rev Immunol*. 2022;40(1):589–614. doi:10.1146/annurev-immunol-093019-125148

5. Bresser PL, Vorster M, Sathekge MM. An overview of the developments and potential applications of 68 Ga-labelled PET/CT hypoxia imaging. *Ann Nucl Med*. 2021;35(2):148–158. doi:10.1007/s12149-020-01563-7
6. Lawal IO, Abubakar S, Ankrah AO, Sathekge MM. Molecular imaging of tuberculosis. *Semin Nucl Med*. 2023;53(1):37–56. doi:10.1053/j.semnuclmed.2022.07.001
7. Veatch AV, Kaushal D. Opening Pandora's Box: mechanisms of Mycobacterium tuberculosis resuscitation. *Trends Microbiol*. 2018;26(2):145–157. doi:10.1016/j.tim.2017.08.001
8. Datta M, Via LE, Kamoun WS, et al. Anti-vascular endothelial growth factor treatment normalizes tuberculosis granuloma vasculature and improves small molecule delivery. *Proc Natl Acad Sci U S A*. 2015;112(6):1827–1832. doi:10.1073/pnas.1424563112
9. Oehlers SH. Revisiting hypoxia therapies for tuberculosis. *Clin Sci*. 2019;133(12):1271–1280. doi:10.1042/CS20190415
10. Batista LAF, Silva KJS, da Costa E Silva LM, et al. Tuberculosis: a granulomatous disease mediated by epigenetic factors. *Tuberculosis*. 2020;123:101943. doi:10.1016/j.tube.2020.101943
11. Cardoso MS, Silva TM, Resende M, Appelberg R, Borges M, Ehrt S. Lack of the transcription factor hypoxia-inducible factor 1α (HIF-1α) in macrophages accelerates the necrosis of mycobacterium avium-induced granulomas. *Infect Immun*. 2015;83(9):3534–3544. doi:10.1128/IAI.00144-15
12. Oehlers SH, Cronan MR, Scott NR, et al. Interception of host angiogenic signalling limits mycobacterial growth. *Nature*. 2015;517(7536):612–615. doi:10.1038/nature13967
13. Pang X, Liu X, Cheng Y, et al. Sono-immunotherapeutic nanocapturer to combat multidrug-resistant bacterial infections. *Adv Mater*. 2019;31(35):e1902530. doi:10.1002/adma.201902530
14. Xu F, Hu M, Liu CC, Choi SK. Yolk-structured multifunctional up-conversion nanoparticles for synergistic photodynamic-sonodynamic antibacterial resistance therapy. *Biomater Sci*. 2017;5(4):678–685. doi:10.1039/C7BM00030H
15. Sun D, Pang X, Cheng Y, et al. Ultrasound-switchable nanozyme augments sonodynamic therapy against multidrug-resistant bacterial infection. *ACS Nano*. 2020;14(2):2063–2076. doi:10.1021/acsnano.9b08667
16. Duo YH, Zhu DM, Sun XR, et al. Patient-derived microvesicles/AIE luminogen hybrid system for personalized sonodynamic cancer therapy in patient-derived xenograft models. *Biomaterials*. 2021;272(1):120755. doi:10.1016/j.biomaterials.2021.120755
17. Dong Y, Su H, Jiang HX, et al. Experimental study on the influence of low-frequency and low-intensity ultrasound on the permeability of the mycobacterium smegmatis cytoderm and potentiation with levofloxacin. *Ultrason Sonochem*. 2017;37:1–8. doi:10.1016/j.ultsonch.2016.12.024
18. Cheng X, He L, Xu JX, et al. Oxygen-producing catalase-based prodrug nanoparticles overcoming resistance in hypoxia-mediated chemo-photodynamic therapy. *Acta Biomater*. 2020;112:234–249. doi:10.1016/j.actbio.2020.05.035
19. Zhang ZF, Zhang YQ, Yang M, et al. Synergistic antibacterial effects of ultrasound combined nanoparticles encapsulated with cellulase and levofloxacin on Bacillus Calmette-Guérin biofilms. *Front Microbiol*. 2023;14:1108064. doi:10.3389/fmicb.2023.1108064
20. Czechowska E, Ranoszek-Soliwoda K, Tomaszewska E, et al. Comparison of the antioxidant activity of catalase immobilized on gold nanoparticles via specific and non-specific adsorption. *Colloids Surf B Biointerfaces*. 2018;171:707–714. doi:10.1016/j.colsurfb.2018.07.036
21. Tiberi S, Zumla A, Migliori GB. Multidrug and extensively drug-resistant tuberculosis: epidemiology, clinical features, management and treatment. *Infect Dis Clin North Am*. 2019;33(4):1063–1085. doi:10.1016/j.idc.2019.09.002
22. Sarathy JP, Zuccotto F, Hsinpin H, et al. Prediction of drug penetration in tuberculosis lesions. *ACS Infect Dis*. 2016;2(8):552–563. doi:10.1021/acsinfecdis.6b00051
23. Mast JM, Kuppusamy P. Hyperoxygenation as a therapeutic supplement for treatment of triple negative breast cancer. *Front Oncol*. 2018;8:527. doi:10.3389/fonc.2018.00527
24. Zhu P, Chen Y, Shi JL. Nanoenzyme-augmented cancer sonodynamic therapy by catalytic tumor oxygenation. *ACS Nano*. 2018;12(4):3780–3795. doi:10.1021/acsnano.8b00999
25. Geng XR, Chen YH, Chen ZY, Wei XY, Dai YL, Yuan Z. Oxygen-carrying biomimetic nanoplatform for sonodynamic killing of bacteria and treatment of infection diseases. *Ultrason Sonochem*. 2022;84:105972. doi:10.1016/j.ultsonch.2022.105972
26. Li GZ, Wang SP, Deng DS, et al. Fluorinated chitosan to enhance transmucosal delivery of sonosensitizer-conjugated catalase for sonodynamic bladder cancer treatment post-intravesical instillation. *ACS Nano*. 2020;14(2):1586–1599. doi:10.1021/acsnano.9b06689
27. Minassian AM, Satti I, Poulton ID, Meyer J, Hill AV, McShane H. A human challenge model for mycobacterium tuberculosis using mycobacterium bovis Bacille Calmette-Guerin. *J Infect Dis*. 2012;205(7):1035–1042. doi:10.1093/infdis/jis012
28. Yang M, Du KY, Hou YR, et al. Synergistic antifungal effect of amphotericin b-loaded poly(lactic-co-glycolic acid) nanoparticles and ultrasound against candida albicans biofilms. *Antimicrob Agents Chemother*. 2019;63(4):e02022–18. doi:10.1128/AAC.02022-18
29. Liu G, Gao NS, Zhou Y, et al. Polydopamine-based "four-in-one" versatile nanoplatforms for targeted dual chemo and photothermal synergistic cancer therapy. *Pharmaceutics*. 2019;11(10):507. doi:10.3390/pharmaceutics11100507
30. Huang XN, Du XY, Xing JF, Ge ZQ. Catalase-only nanoparticles prepared by shear alone: characteristics, activity and stability evaluation. *Int J Biol Macromol*. 2016;90:81–88. doi:10.1016/j.ijbiomac.2015.08.056
31. Schön T, Werngren J, Machado D, et al. Antimicrobial susceptibility testing of Mycobacterium tuberculosis complex isolates–the EUCAST broth microdilution reference method for MIC determination. *Clin Microbiol Infect*. 2020;26(11):1488–1492. doi:10.1016/j.cmi.2020.07.036
32. Fenaroli F, Repnik U, Xu YT, et al. Enhanced permeability and retention-like extravasation of nanoparticles from the vasculature into tuberculosis granulomas in zebrafish and mouse models. *Acs nano*. 2018;12(8):8646–8661. doi:10.1021/acsnano.8b04433
33. Zhang R, Song XJ, Liang C, et al. Catalase-loaded cisplatin-prodrug-constructed liposomes to overcome tumor hypoxia for enhanced chemo-radiotherapy of cancer. *Biomaterials*. 2017;138:13–21. doi:10.1016/j.biomaterials.2017.05.025
34. Song GS, Chen YY, Liang C, et al. Catalase-loaded TaOx nanoshells as bio-nanoreactors combining high-z element and enzyme delivery for enhancing radiotherapy. *Adv Mater*. 2016;28(33):7143–7148. doi:10.1002/adma.201602111
35. Drlica K, Zhao X. Bacterial death from treatment with fluoroquinolones and other lethal stressors. *Expert Rev Anti Infect Ther*. 2021;19(5):601–618. doi:10.1080/14787210.2021.1840353
36. Yang H, Song L, Sun P, et al. Synergistic bactericidal effect of ultrasound combined with citral nanoemulsion on Salmonella and its application in the preservation of purple kale. *Ultrason Sonochem*. 2023;92:106269. doi:10.1016/j.ultsonch.2022.106269
37. Domingo-Gonzalez R, Das S, Griffiths KL, et al. Interleukin-17 limits hypoxia-inducible factor 1α and development of hypoxic granulomas during tuberculosis. *JCI Insight*. 2017;2(19):e92973. doi:10.1172/jci.insight.92973

38. de Oliveira Rezende A, Sabóia RS, da Costa AC, et al. Restricted activation of the NF-κB pathway in individuals with latent tuberculosis infection after HIF-1α blockade. *Biomedicines*. 2022;10(4):817. doi:10.3390/biomedicines10040817
39. Uusi-Mäkelä M, Rämet M. Hijacking host angiogenesis to drive mycobacterial growth. *Cell Host Microbe*. 2018;24(4):465–466. doi:10.1016/j.chom.2018.09.016
40. Kang YJ, Jo JO, Ock MS, et al. Over-expression of thymosin β4 in granulomatous lung tissue with active pulmonary tuberculosis. *Tuberculosis*. 2014;94(3):323–331. doi:10.1016/j.tube.2014.01.003
41. Piotrowski WJ, Kiszałkiewicz J, Pastuszak-Lewandoska D, et al. Expression of HIF-1α/VEGF/ING-4 axis in pulmonary sarcoidosis. *Adv Exp Med Biol*. 2015;866:61–69.
42. Jain T, Nikolopoulou EA, Xu Q, Qu A. Hypoxia inducible factor as a therapeutic target for atherosclerosis. *Pharmacol Ther*. 2018;183:22–33. doi:10.1016/j.pharmthera.2017.09.003
43. Zhang Z, Yao L, Yang J, Wang Z, Du G. PI3K/Akt and HIF-1 signaling pathway in hypoxia-ischemia (Review). *Mol Med Rep*. 2018;18(4):3547–3554. doi:10.3892/mmr.2018.9375
44. Carmeliet P, Jain RK. Principles and mechanisms of vessel normalization for cancer and other angiogenic diseases. *Nat Rev Drug Discov*. 2011;10(6):417–427. doi:10.1038/nrd3455
45. Zou JJ, Yuan DP, Yang J, Yu Y. Effects of diosmin on vascular leakage and inflammation in a mouse model of venous obstruction. *Front Nutr 2022*. 2022;9:831485. doi:10.3389/fnut.2022.831485
46. Xu YT, Wang LH, Zimmerman MD, et al. Matrix metalloproteinase inhibitors enhance the efficacy of frontline drugs against mycobacterium tuberculosis. *PLoS Pathog*. 2018;14(4):e1006974. doi:10.1371/journal.ppat.1006974
47. Attia SK, Moftah NH, Abdel-Azim ES. Expression of IFN-γ, IL-4, and IL-17 in cutaneous schistosomal granuloma. *Int J Dermatol*. 2014;53(8):991–998. doi:10.1111/ijd.12464
48. Resende M, Cardoso MS, Fróis-Martins R, et al. TNF-mediated compensatory immunity to mycobacterium avium in the absence of macrophage activation by IFN-γ. *J Immunol*. 2019;203(9):2451–2458. doi:10.4049/jimmunol.1801594
49. Boggaram V, Gottipati KR, Wang X, Samten B. Early secreted antigenic target of 6 kDa (ESAT-6) protein of Mycobacterium tuberculosis induces interleukin-8 (IL-8) expression in lung epithelial cells via protein kinase signaling and reactive oxygen species. *J Biol Chem*. 2013;288(35):25500–25511. doi:10.1074/jbc.M112.448217
50. Ochs HD, Oukka M, Torgerson TR. Th17 cells and regulatory T cells in primary immunodeficiency diseases. *J Allergy Clin Immunol*. 2009;123(5):977–985. doi:10.1016/j.jaci.2009.03.030
51. Li X, Guo DX, Hu YD, Chen Y. Evaluation of oxidative status in elderly patients with multiple cerebral infarctions and multiple chronic total coronary occlusions. *Dis Markers*. 2022;2022:2083990. doi:10.1155/2022/2083990
52. Jelic MD, Mandic AD, Maricic SM, Srdjenovic BU. Oxidative stress and its role in cancer. *J Cancer Res Ther*. 2021;17(1):22–28. doi:10.4103/jcrt.JCRT_862_16
53. WS O, Chen H, Chow PH. Male genital tract antioxidant enzymes--their ability to preserve sperm DNA integrity. *Mol Cell Endocrinol*. 2006;250(1–2):80–83. doi:10.1016/j.mce.2005.12.029
54. Wan Y, Xu WZ, Ren X, Wang Y, Dong B, Wang L. Microporous frameworks as promising platforms for antibacterial strategies against oral diseases. *Front Bioeng Biotechnol*. 2020;8:628. doi:10.3389/fbioe.2020.00628
55. Tan H, Tian Y, Yang H, et al. Oxygen-sufficient lipid nanobubbles combined with UTMD for enhanced sonodynamic therapy of Hep-G2 cells. *J Biomed Mater Res B Appl Biomater*. 2021;109(11):1796–1806. doi:10.1002/jbm.b.34839